Solid Freeform Fabrication 2022: Proceedings of the 33rd Annual International
Solid Freeform Fabrication Symposium – An Additive Manufacturing Conference
Reviewed Paper

EVALUATION OF FUNCTIONALLY GRADED LATTICE PROPERTIES OF LASER POWDER BED FUSED STAINLESS STEEL 316L

B. B. Ravichander, S.H. Jagdale, S. Theeda, G. Kumar

Department of Mechanical Engineering, The University of Texas at Dallas, Richardson, TX 75080

Abstract

The development of metal Additive Manufacturing (AM) techniques, in particular the laser powder bed fusion (LPBF) process, has led to an increase in the innovative design and fabrication of lightweight and complex porous metal structures. Despite the limitations of the LPBF process which limits the geometric accuracy of the porous structures, it eliminates the difficulties presented by conventional manufacturing techniques in the fabrication of highly complex structures. The properties of as-built porous structures depend on the unit cell design and porosity level. These lightweight metal structures have applications in medical and aerospace fields. The relationships between the lattice geometry and performance must be determined to successfully implement the functional lattice designs. In this study, functionally graded lattice structures are fabricated from steel using SLM technique and the effect of different lattice types on the manufacturability, density and mechanical properties are investigated.

Keywords: Laser Powder Bed Fusion, Functionally Graded Lattice, Porosity, SS316L, Part Density

1. INTRODUCTION

Stainless steel 316L (316L), is an austenitic steel composed of chromium-nickel-molybdenum alloy [1, 2]. 316L is known for its excellent corrosion resistance, oxidation resistance and low neutron absorption rate [3]. 316L is one of the most widely used structural materials because of good formability, mechanical strength, and fracture toughness [4, 5]. In addition to structural applications, 316L is also used in orthopedic implants, petrochemical, and nuclear power plants [3]. The mechanical properties and the corrosion resistance of 316L depend on the processing technique [6]. The geometrical complexity of metal parts in new applications is constantly increasing and the conventional manufacturing techniques like machining, casting, and forging are not suitable to meet the demand [7]. The advances in computer aided design (CAD) have led to new design opportunities like topology optimization that enables reduction in part weight without compromising the performance. Due to the changes in the design and the desired properties, there is a need for the microstructure and mechanical properties to be controlled at various levels. Therefore, AM offers a viable alternative to conventional manufacturing techniques [8, 9].

LPBF is a layer-by-layer manufacturing process capable of fabricating highly dense parts with complex geometries [10-14]. The LPBF process uses a recoater to deposit metal powder on the substrate. The powder is then melted and fused with the help of a laser heat source. The process is continued till the entire geometry of the part is fabricated [14-16] . LPBF process has the ability

to fabricate specimens with varying porosities and complex shapes. The LPBF fabricated parts can achieve microstructures and properties comparable to the cast counterparts under optimized processing conditions. The customized microstructures and properties can be achieved by tailoring the process parameters and thus process optimization studies are still being carried out for solid parts from different alloys [17]. Triply periodic minimal surfaces (TPMS), honeycomb are some of the examples of porous metal structures that are desirable for applications in aerospace, automobile, heat exchangers but their fabrication strategies are not well established [18]. The porous structures consist of multiple pores organized in unit cell configurations throughout the volume of the specimen. The design of the TPMS structures is slightly complicated as they are mathematically defined surfaces, while the lattices and the honeycomb structures can be easily designed with the help of various CAD packages [19].

Gibson *et al.*, developed a model known as the Gibson-Ashby model to determine the relative density based on the lattice structure's theoretical mechanical properties [20]. Zhang *et al.* used SLM technique to fabricate 316L TPMS structures and studied their mechanical and energy absorption capabilities [21]. Abueidda *et al.*, studied the effect of porosity levels on the mechanical properties of Selectively laser sintering (SLS) fabricated specimens [22]. In a similar study, Yang *et al.*, compared the experimental values of elastic modulus and yield strength of SLM fabricated Ti64Al4V samples with that of finite element simulations [23]. Numerous studies have been conducted to examine the correlation between the porosity grading methodologies and the physical properties [24-26]. Functionally graded diamond-type lattice structures and their mechanical properties were studied by Han *et al* [24]. It was observed that the diamond structured lattice failed layer by layer as opposed to the diagonal shear band that is commonly observed in compressively loaded homogenous lattices [24] . Similar results were observed on the functionally graded 316L gyroid lattice [27]. Wang *et al.*, investigated the effect of varying cell sizes on the mechanical properties of SLM fabricated Ti6Al4V alloy [28]. It was found that the stress-strain responses revealed a post-peak significant drop in the strength. To our knowledge, no comprehensive study has been done to compare different functionally graded porous metal lattice fabricated by 3D printing. In this work, different functionally graded TPMS structures are designed from 316L using SLM Solutions 125 HL printer. Compressive tests were performed on the as-built 316L lattices to determine the mechanical properties of the TPMS structures. Part densities of the samples were measured and their effect on the mechanical properties was evaluated.

2. MATERIALS AND METHODS

2.1 Design of Lattice Structures

A total of 5 TPMS structures (i.e., Diamond, Gyroid, Primitive, Neovius, and Fisher-Koch S) were designed with the help of MS Lattice, an open source TPMS surface generator [29] as shown in Figure 1. The total size of the samples was maintained at 8 mm x 8 mm x 8 mm with each unit cell being 2 mm x 2 mm x 2 mm. The porosity of the samples was varied from 30% to 70%. The TPMS were then converted into 3D stereo-lithography (STL) files. The STL files were imported into Solidworks (Dassault Systèmes, Vélizy-Villacoublay, France) and two plates (each with the thickness of 1 mm) were added at the top and bottom of the porous structures to support the mechanical testing. The Solidworks files were imported to Materialise Magics (© Copyright Materialise 2021, Leuven, Belgium) to assign the supports and corresponding process parameters

for printing. Equations 1-5 represent the nodal approximations of the TPMS structures where constant K governs the porosity:

Diamond	$f(x,y,z) = sin(x) * sin(y) * sin(z) + sin(x) * cos(y) * cos(z) + cos(x) * sin(y) * cos(z) + cos(x) * cos(y) * sin(z) - K$	Equation 1
Gyroid	$f(x,y,z) = sin(x) * cos(y) + sin(y) * cos(z) + sin(z) * cos(x) - K$	Equation 2
Primitive	$f(x,y,z) = cos(x) + cos(y) + cos(z) - K$	Equation 3
Neovius	$f(x,y,z) = 3 * (cos(x) + cos(y) + cos(z)) + 4 * cos(x) * cos(y) * cos(z) - K$	Equation 4
Fisher-Koch S	$f(x,y,z) = cos(2x) * sin(y) * cos(z) + cos(2y) * sin(z) * cos(x) + cos(2z) * sin(x) * cos(y) - K$	Equation 5

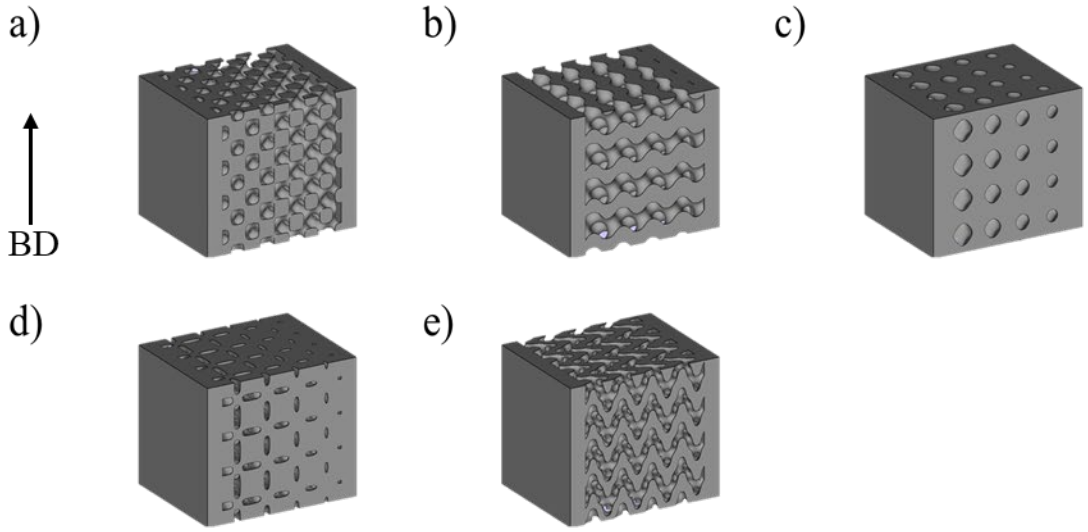

Figure 1. Designed TPMS structures with varying porosity levels from 30% to 70% and build direction (BD) indicated by the arrow and types: a) Diamond; b) Gyroid; c) Primitive; d) Neovius; e) Fisher-Koch S.

2.2 Powder Preparation and Fabrication

The 316L TPMS specimens were fabricated using SLM 125 HL LPBF printer (SLM Solutions Group AG, Lübeck, Germany). The SLM 125 HL LPBF printer is equipped with a 400 W Ytterbium fiber laser and has a build volume of 125mm×125mm×125mm. Gas atomized 316L powder was obtained from SLM solutions AG. Figure 2 shows the scanning electron microscope

(SEM) micrograph of the fresh 316L powder, and its composition is listed in Table 1. From the SEM micrograph it can be seen that the powder particles are mostly spherical.

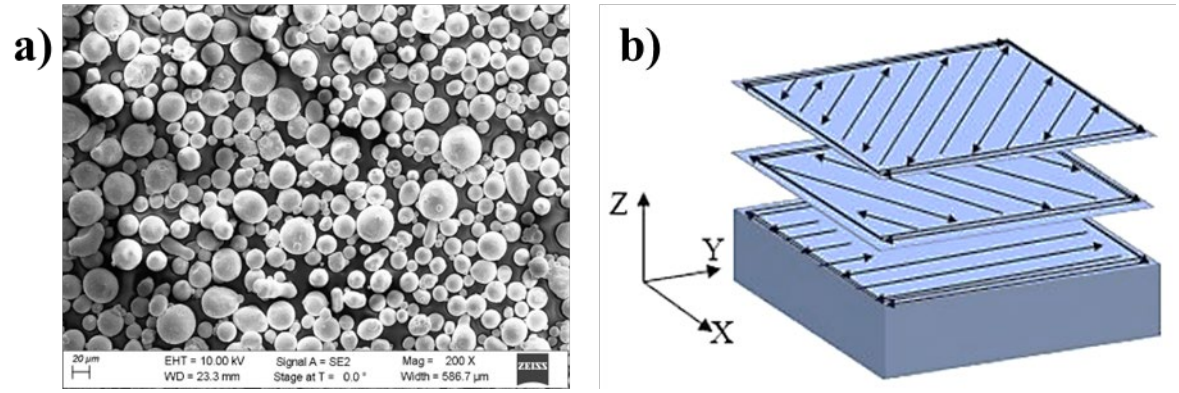

Figure 2. a) SEM micrograph of fresh 316L powder used during fabrication and b) Schematic depicting the stripes scan strategy used during the SLM process.

Table 1: The chemical composition of 316L powder obtained from SLM Solutions.

Element	Fe	Cr	Ni	Mo	Nb + Ta	Mn	Si	P	S	C	N	O
Mass fraction (%)	Balance	16-18	10-14	2-3	-	2	1	0.045	0.03	0.03	0.1	-

The samples were fabricated with the SLM Solutions suggested process parameter set. The laser power (LP = 200 W), scan speed (SS = 800 mm/s), hatch spacing (HS = 120 µm), layer thickness (LT = 30 µm) and the stripes scan strategy as displayed in figure 2 were employed for the fabrication of TPMS samples. The energy density (E_v) used during the fabrication process is: 69.45 J/mm^3 calculated using equation [9, 11, 15, 16]:

$$E_v = \frac{LP}{SS \times HS \times LT} \qquad \text{Equation 6}$$

2.3 Experimental Procedure

A wire electrical discharge machine was used to remove the as-built samples from the stainless-steel substrate. Density measurements were performed using the Archimedes method. The samples were first weighed in air with the help of a Precision Balance. The samples were later measured in water and the density was calculated. The quasi-static compression tests were performed at room temperature using an Instron 6559 universal testing machine equipped with a 50 kN load cell. A constant strain rate of 10^{-2} sec^{-1} was applied perpendicular to the build direction. The maximum displacement allowed for each sample was limited to 50% or 5 mm due to use of the 50 kN load cell.

3. Results and Discussion

3.1 Part Density Analysis

The mechanical properties of the TPMS specimens depend significantly on the density of the fabricated surface. Figure 3 shows the part density values for the fabricated TPMS specimens. The highest part density values were found for the Fisher-Koch S (98.77%) lattice followed by the Diamond (97.85%) and Gyroid (97.69%) lattices. The Neovius and the primitive lattice structures yielded comparatively lower part density values of 96.28% and 93.31% respectively. The achievement of near fully dense samples is usually expected from the LPBF process as they are capable of fabricating samples with complex geometries. The samples were fabricated with the optimized processing parameters for 316L as suggested by the SLM solutions, given in Section 2.2. The functionally graded porosities seem to have an impact on the density, and it must be noted that the process parameters and scan strategy play a significant role in determining the density of the fabricated specimens [30]. Therefore, it is important to establish the effect of these processing parameters on the part density of functionally graded lattice in future research. Due to the functionally graded nature of the fabricated specimens and the small unit cell size of 2 mm, it was noticed that the part density values were significantly lower and reduced the manufacturability of these samples as reported by Rajgopalan *et al.* [31]. The lower part density values can also be due to shrinkage, lack of fusion between powder particles and other defects such as unmelted powder particles. This can be observed at the more porous regions of the sample (70% porous side) as it had bigger overhang sections and deformation due to thermal stresses [32, 33].

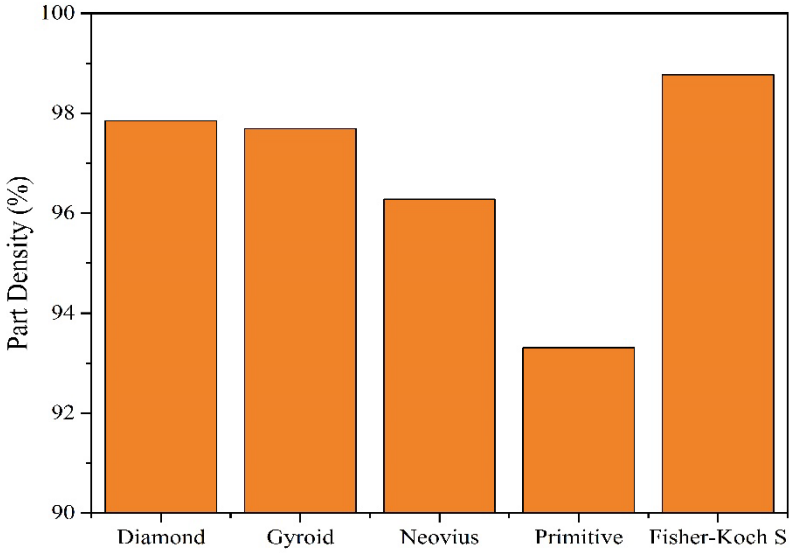

Figure 3. Part densities of the 316L TPMS specimens with same unit cell size of 2mm.

3.2 Quasi-Static Compression Testing

The part density and unit cell type of the functionally graded lattice specimens govern the mechanical properties. The stress-strain curves of as-built TPMS samples are shown in Figure 4. The tests were performed with the loading direction perpendicular to the build direction (See Figure 1). The Young's modulus was obtained by calculating the slope of the elastic region and the compressive yield strength of samples was determined by using 0.2% offset approach [32]. The stress-strain curves indicate that after the initial elastic region, the structures deform plastically and continue to absorb energy. This is followed by the densification stage, where the samples behave similar to that of solid material as there is a large self-contact area as seen in Figure 6. A similar trend was observed in a study conducted by Li *et al.* [33]. From Figure 5, we can see that the Fisher-Koch S specimen had the highest Young's modulus value of 5.12 GPa followed by the

Diamond (4.51 GPa) and Gyroid (4.21 GPa) lattice samples. The Primitive and Neovius structues resulted in lower Young's modulus values of 2.48 GPa and 2.13 GPa respectively. However, the compressive yield strength was highest for the primitive structure (112.83 MPa) followed by the Fisher-Koch S (98.66 MPa) sample. The diamond and gyroid samples had slightly lower yield strength values of 80.41 MPa and 69.47 MPa. The neovius structure resulted in the lowest yield strength value of 42.52 MPa. The experimental deformation of the samples at different strains is presented in Figure 6. The samples did not deform with a diagonal shear but rather deformed layer by layer as in the case for uniformly graded lattices [24, 27].

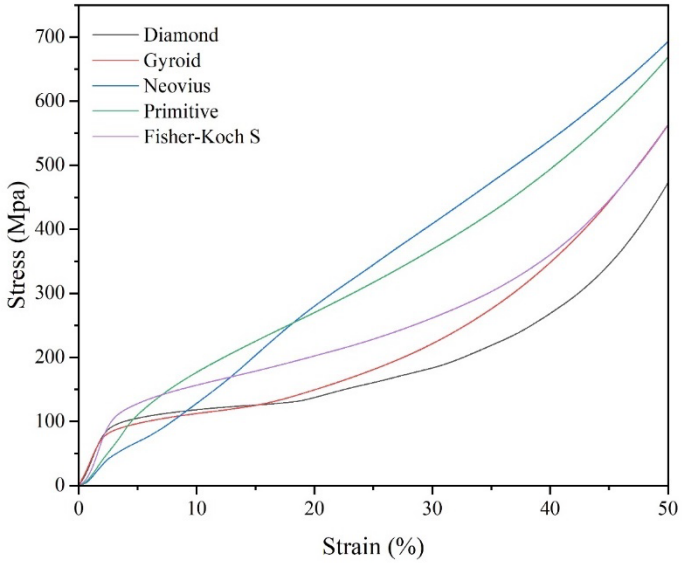

Figure 4. Stress-Strain curves of the different as-fabricated functionally graded lattice specimens.

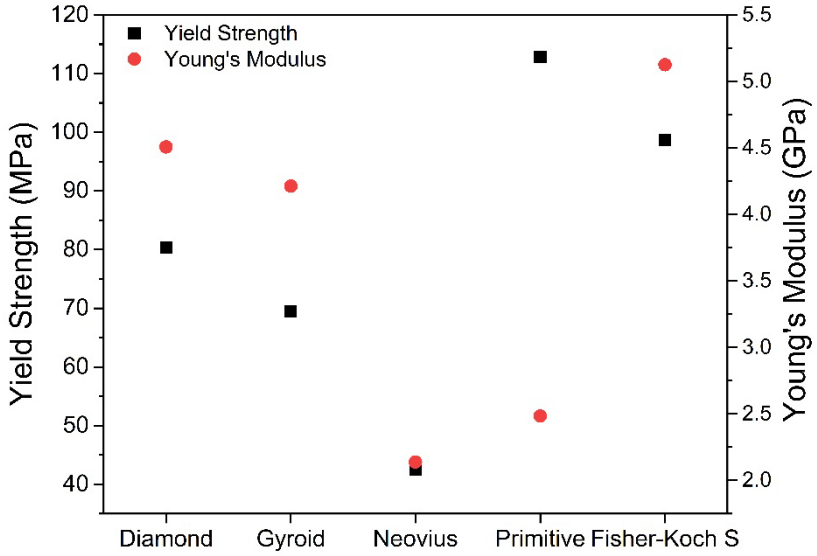

Figure 5. Young's Modulus and yield strength values of the different as-fabricated functionally graded lattice specimens.

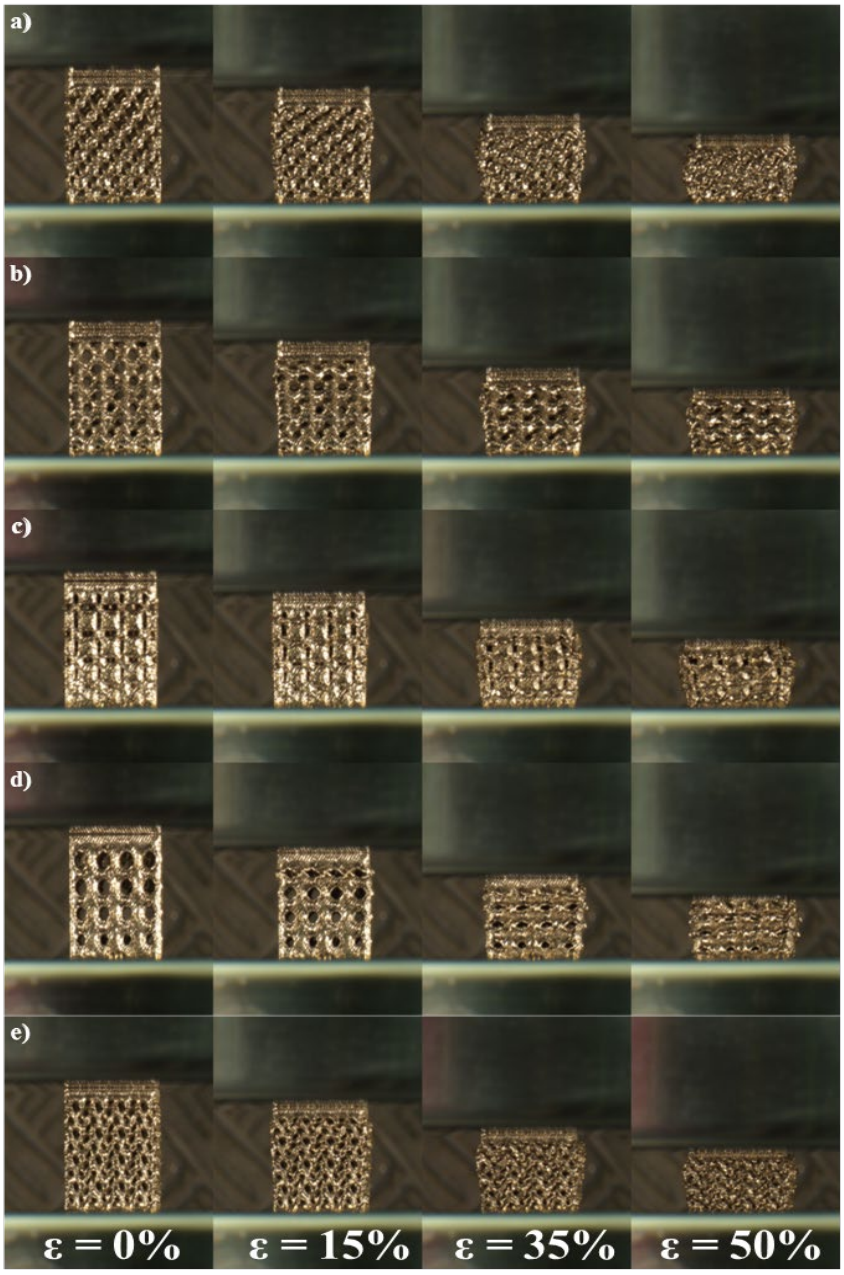

Figure 6. Experimental deformation of a) Diamond, b) Gyroid, c) Neovius, d) Primitive, and e) Fisher-Koch S at different strains.

4. CONCLUSION

In this study, functionally graded lattice 316L structures with porosity varying from 30% to 70% were designed and fabricated using the LPBF technique. The fabricated lattice specimens were evaluated on part density and quasi-static compression behavior. The part density of the Fisher-Koch S, Diamond and Gyroid lattice samples were closer to the desired part density with no internal voids i.e., 100% dense. The Primitive lattice sample had the lowest part density value. The primitive structure resulted in a higher compressive yield strength value of 112.834 MPa. On the contrary, it had a low Young's modulus of 2.485 GPa. The fisher-Koch S sample resulted in a high

value for Young's modulus (5.1255 GPa) and had the second highest yield strength (98.66 MPa) value.

5. ACKNOWLEDGEMENT

This work was supported by a University of Texas System STARs award.

6. REFERENCES

[1] M. Ghayoor, K. Lee, Y. He, C.-h. Chang, B.K. Paul, S. Pasebani, Selective laser melting of 304L stainless steel: Role of volumetric energy density on the microstructure, texture and mechanical properties, Additive Manufacturing 32 (2020) 101011.
[2] M. Laleh, A.E. Hughes, W. Xu, I. Gibson, M.Y. Tan, Unexpected erosion-corrosion behaviour of 316L stainless steel produced by selective laser melting, Corrosion Science 155 (2019) 67-74.
[3] S. Mohd Yusuf, Y. Chen, S. Yang, N. Gao, Microstructural evolution and strengthening of selective laser melted 316L stainless steel processed by high-pressure torsion, Materials Characterization 159 (2020) 110012.
[4] W. Fredriksson, D. Petrini, K. Edström, F. Björefors, L. Nyholm, Corrosion resistances and passivation of powder metallurgical and conventionally cast 316L and 2205 stainless steels, Corrosion Science 67 (2013) 268-280.
[5] A.B. Kale, B.-K. Kim, D.-I. Kim, E.G. Castle, M. Reece, S.-H. Choi, An investigation of the corrosion behavior of 316L stainless steel fabricated by SLM and SPS techniques, Materials Characterization 163 (2020) 110204.
[6] N. Kurgan, Y. Sun, B. Cicek, H. Ahlatci, Production of 316L stainless steel implant materials by powder metallurgy and investigation of their wear properties, Chinese Science Bulletin 57(15) (2012) 1873-1878.
[7] S. Srihari, B.R. Bharath, M. Narges Shayesteh, S. Nahid, A. Amirhesam, Investigation of the strength of different porous lattice structures manufactured using selective laser melting, Proc.SPIE, 2020.
[8] R. Bharath Bhushan, A. Amirhesam, M. Narges Shayesteh, Toward mitigating microcracks using nanopowders in laser powder bed fusion, Proc.SPIE, 2021.
[9] R. Bharath Bhushan, F. Carolina, A. Amirhesam, M. Narges Shayesteh, A framework for the optimization of powder-bed fusion process, Proc.SPIE, 2021.
[10] B. Farhang, B.B. Ravichander, F. Venturi, A. Amerinatanzi, N. Shayesteh Moghaddam, Study on variations of microstructure and metallurgical properties in various heat-affected zones of SLM fabricated Nickel–Titanium alloy, Materials Science and Engineering: A 774 (2020) 138919.
[11] B.B. Ravichander, A. Amerinatanzi, N. Shayesteh Moghaddam, Study on the Effect of Powder-Bed Fusion Process Parameters on the Quality of as-Built IN718 Parts Using Response Surface Methodology, Metals 10(9) (2020).
[12] B. Farhang, B.B. Ravichander, J. Ma, A. Amerinatanzi, N. Shayesteh Moghaddam, The evolution of microstructure and composition homogeneity induced by borders in laser powder bed fused Inconel 718 parts, Journal of Alloys and Compounds 898 (2022) 162787.
[13] B.B. Ravichander, K. Mamidi, V. Rajendran, B. Farhang, A. Ganesh-Ram, M. Hanumantha, N. Shayesteh Moghaddam, A. Amerinatanzi, Experimental investigation of laser scan strategy on the microstructure and properties of Inconel 718 parts fabricated by laser powder bed fusion, Materials Characterization 186 (2022) 111765.

[14] B.B. Ravichander, S. Thakare, A. Ganesh-Ram, B. Farhang, M. Hanumantha, Y. Yang, N. Shayesteh Moghaddam, A. Amerinatanzi, Cost-Aware Design and Fabrication of New Support Structures in Laser Powder Bed Fusion: Microstructure and Metallurgical Properties, Applied Sciences 11(21) (2021).
[15] R. Bharath Bhushan, F. Behzad, S. Nahid, A. Amirhesam, M. Narges Shayesteh, Analysis of the deviation in properties of selective laser melted samples fabricated by varying process parameters, Proc.SPIE, 2020.
[16] B.B. Ravichander, A. Rahimzadeh, B. Farhang, N. Shayesteh Moghaddam, A. Amerinatanzi, M. Mehrpouya, A Prediction Model for Additive Manufacturing of Inconel 718 Superalloy, Applied Sciences 11(17) (2021).
[17] E. Liverani, S. Toschi, L. Ceschini, A. Fortunato, Effect of selective laser melting (SLM) process parameters on microstructure and mechanical properties of 316L austenitic stainless steel, Journal of Materials Processing Technology 249 (2017) 255-263.
[18] L.J. Gibson, M.F. Ashby, Cellular solids : structure and properties, Cambridge, New York, 1997.
[19] L. Han, S. Che, An Overview of Materials with Triply Periodic Minimal Surfaces and Related Geometry: From Biological Structures to Self-Assembled Systems, Advanced Materials 30(17) (2018) 1705708.
[20] L.J. Gibson, Cellular Solids, MRS Bulletin 28(4) (2003) 270-274.
[21] L. Zhang, S. Feih, S. Daynes, S. Chang, M.Y. Wang, J. Wei, W.F. Lu, Energy absorption characteristics of metallic triply periodic minimal surface sheet structures under compressive loading, Additive Manufacturing 23 (2018) 505-515.
[22] D.W. Abueidda, M. Bakir, R.K. Abu Al-Rub, J.S. Bergström, N.A. Sobh, I. Jasiuk, Mechanical properties of 3D printed polymeric cellular materials with triply periodic minimal surface architectures, Materials & Design 122 (2017) 255-267.
[23] L. Yang, C. Yan, C. Han, P. Chen, S. Yang, Y. Shi, Mechanical response of a triply periodic minimal surface cellular structures manufactured by selective laser melting, International Journal of Mechanical Sciences 148 (2018) 149-157.
[24] C. Han, Y. Li, Q. Wang, S. Wen, Q. Wei, C. Yan, L. Hao, J. Liu, Y. Shi, Continuous functionally graded porous titanium scaffolds manufactured by selective laser melting for bone implants, Journal of the Mechanical Behavior of Biomedical Materials 80 (2018) 119-127.
[25] K.F. Leong, C.K. Chua, N. Sudarmadji, W.Y. Yeong, Engineering functionally graded tissue engineering scaffolds, Journal of the Mechanical Behavior of Biomedical Materials 1(2) (2008) 140-152.
[26] M. Afshar, A. Pourkamali Anaraki, H. Montazerian, Compressive characteristics of radially graded porosity scaffolds architectured with minimal surfaces, Materials Science and Engineering: C 92 (2018) 254-267.
[27] L. Yang, R. Mertens, M. Ferrucci, C. Yan, Y. Shi, S. Yang, Continuous graded Gyroid cellular structures fabricated by selective laser melting: Design, manufacturing and mechanical properties, Materials & Design 162 (2019) 394-404.
[28] S. Wang, Z.a. Shi, L. Liu, X. Zhou, L. Zhu, Y. Hao, The design of Ti6Al4V Primitive surface structure with symmetrical gradient of pore size in biomimetic bone scaffold, Materials & Design 193 (2020) 108830.
[29] O. Al-Ketan, R.K. Abu Al-Rub, MSLattice: A free software for generating uniform and graded lattices based on triply periodic minimal surfaces, Material Design & Processing Communications 3(6) (2021) e205.

[30] J.P. Kruth, S. Kumar, J. Van Vaerenbergh, Study of laser-sinterability of ferro-based powders, Rapid Prototyping Journal 11(5) (2005) 287-292.
[31] S. Rajagopalan, R.A. Robb, Schwarz meets Schwann: Design and fabrication of biomorphic and durataxic tissue engineering scaffolds, Medical Image Analysis 10(5) (2006) 693-712.
[32] A. Yánez, A. Herrera, O. Martel, D. Monopoli, H. Afonso, Compressive behaviour of gyroid lattice structures for human cancellous bone implant applications, Materials Science and Engineering: C 68 (2016) 445-448.
[33] X. Li, L. Xiao, W. Song, Compressive behavior of selective laser melting printed Gyroid structures under dynamic loading, Additive Manufacturing 46 (2021) 102054.